Mesoscopic and microscopic phase segregation in manganese perovskites

P. G. Radaelli,[1] R. M. Ibberson,[1] D. N. Argyriou,[2] H. Casalta,[3] K. H. Andersen,[3,*] S.-W. Cheong,[4,5] and J. F. Mitchell[2]
[1]*ISIS facility, Rutherford Appleton Laboratory-CCLRC, Chilton, Didcot, Oxfordshire, OX11 0QX, United Kingdom*
[2]*Materials Science Division, Argonne National Laboratory, Argonne, Illinois 60439*
[3]*Institut Max Von Laue–Paul Langevin, BP 156, F-38042 Grenoble Cedex 9, France*
[4]*Department of Physics and Astronomy, Rutgers University, Piscataway, New Jersey 08855*
[5]*Bell Laboratories, Lucent Technologies, Murray Hill, New Jersey 07974*
(Received 20 September 2000; published 16 April 2001)

Mesoscopic (500–2000 Å) and microscopic (5–20 Å) phase segregation with temperature and magnetic field was studied in the model manganite $Pr_{0.7}Ca_{0.3}MnO_3$ by high-resolution neutron diffraction and inelastic neutron scattering. Intragranular strain-driven mesoscopic segregation between two insulating phases, one of which is charge ordered (CO), sets in below the CO temperature in zero field. The CO phase orders antiferromagnetically, while the other insulating phase shows spin-glass behavior. After field-induced metallization, the CO phase coexists with a ferromagnetic metallic phase.

DOI: 10.1103/PhysRevB.63.172419 PACS number(s): 75.30.Vn, 61.12.−q

The issue of phase segregation (PS) has recently come to the forefront of the discussion in the field of manganites, both in theory and experiments. Although PS in manganites was already hypothesized by De Gennes[1] in 1960, recent PS models directly stem from the application of computational techniques to the double-exchange/ferromagnetic Kondo lattice theory.[2] In these models, some charge densities could not be stabilized, leading to an inhomogeneous ground state.[3] One of the two coexisting phases is a ferromagnetic (FM) metal, while the other is an insulator. This type of electronic phase segregation cannot become long-range, due to the high Coulomb energy cost. Therefore, a *microscopically inhomogeneous* state develops, whereby FM clusters, 10–20 Å in diameter, are interspersed into a charge-localized ''matrix,'' the latter associated with much larger lattice distortions than the former, due to the Jahn-Teller effect. The PS scenario bridges the gap between double exchange-type models, which do not take lattice energy into account, and more recent polaronic models,[4] where lattice distortions are treated as associated with a single charge. Microscopic phase segregation is now supported by significant experimental evidence,[2] in particular from neutron scattering.[5,6] At the same time, a number of experimental papers have shown, in the ''narrow-bandwidth'' region of the phase diagram,[7] phase coexistence at a much larger length scale (300–2000 Å) in perovskites[8,9] and, more recently, in layered manganites.[10] Until now, the more or less implicit assumption has been that this *mesoscopic phase segregation* is similar in nature and in origin to the microscopic one, arising from the very close energetic proximity between a FM metallic phase and an insulating phase.

The narrow-bandwidth manganese perovskite $Pr_{0.7}Ca_{0.3}MnO_3$ provides perhaps the best-known example of ''tunable'' mesoscopic phase segregation.[8,11] In fact, its transport and magnetic properties can be dramatically altered by an external action. In zero field, $Pr_{0.7}Ca_{0.3}MnO_3$ undergoes a charge-ordering (CO) transition at $T_{CO} \sim 180-210$ K, to a more disordered variant of the ''*C-E*'' phase[8,12] (found, for instance, in $La_{0.5}Ca_{0.5}MnO_3$), accompanied by a sharp upturn of the resistivity curve.[13] Upon further cooling, AFM order sets in at $T_N \sim 140$ K, with a FM component developing at $T_C \sim 80-100$ K, long interpreted as arising from spin canting,[12] while the electrical resistivity continues to rise. $Pr_{0.7}Ca_{0.3}MnO_3$ can be irreversibly turned into a FM metal by application of an external magnetic field,[14,15] pressure[13] or illumination with x-ray radiation at low temperatures.[8,16] The pristine properties can be recovered by warming above 100 K.[5] This compound is an appealing test system, because chemical disorder should be minimal (Ca^{+2} and Pr^{+3} have almost identical ionic radii). Also, unlike the La-substituted analogues,[9,17] $Pr_{0.7}Ca_{0.3}MnO_3$ has low lattice degeneracy (the three orthorhombic lattice parameters are significantly different), which is a considerable advantage for high-resolution powder diffraction studies. We have reexamined this compound by means of high-resolution neutron powder diffraction (hr-NPD), which enabled us to determine the structural, magnetic and (by inference) electronic properties of *each* of the coexisting mesoscopic phases across a significant portion of the phase diagram. We also determined the local magnetic static and dynamic correlations (a good indicator of microscopic PS) by quasi-elastic small angle neutron scattering (QESANS). Our conclusion is that the two types of PS have different origins. Mesoscopic PS arises primarily from the need to minimize intragranular lattice strain, and was found to occur either between two charge-localized phases or between a metal and an insulator.

A polycrystalline sample of $Pr_{0.7}Ca_{0.3}MnO_3$ was prepared using a standard ceramic route. hr-NPD data ($\Delta d/d \leqslant 0.1\%$ for $0.7\,\text{Å} \leqslant d \leqslant 2.4\,\text{Å}$) were obtained on the diffractometer HRPD at ISIS. The simultaneous use of the three detector banks gave a continuous coverage in the range $0.7\,\text{Å} \leqslant d \leqslant 12.2\,\text{Å}$, which includes all the magnetic reflections. Two series of measurements, all in zero applied magnetic field, were performed (the HRPD detector technology does not permit to measure in an applied field). In the first series, data were collected at various temperatures on *cooling* from room temperature to 3 K. In the second series, data were collected on warming from 3 K, after the application of an external magnetic field of 7 T for 4 h, followed by ramp-down to zero field. Data sets were also collected at 3 K after the application of intermediate field values, confirming that an irreversible transition to a FM state occurs above 5 T (see below).

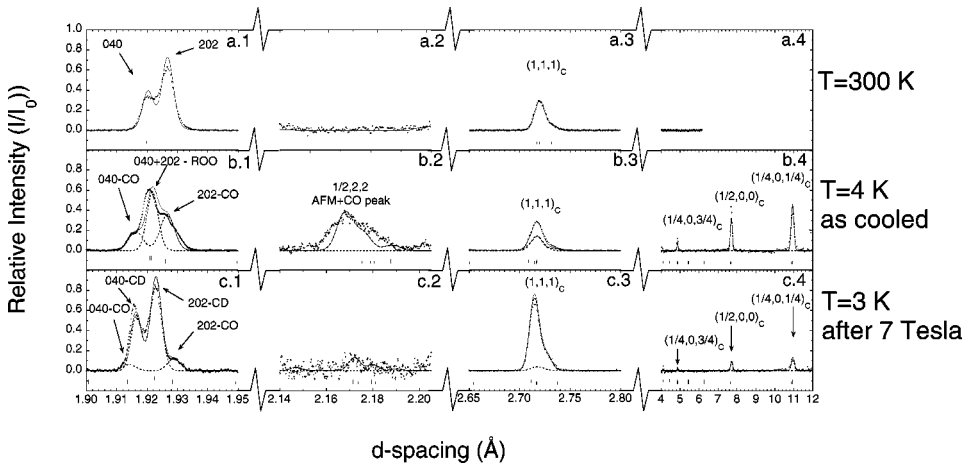

FIG. 1. Phase segregation in $Pr_{0.7}Ca_{0.3}MnO_3$ from nuclear and magnetic high-resolution neutron powder diffraction data at room temperature (a1)–(a4), 4 K after zero-field cooling (b1)–(b4) and 3 K after application of a 7 T magnetic field followed by ramp-down to zero field. The data, normalized to the scattering of a 6 mm vanadium rod, were originally on the same dimensionless intensity scale, but were normalized to 1 for multiplotting. (a1)–(c1): ($I_0 = 0.03$) The nuclear 040-202 doublet (orthorhombic lattice constants $\sim\sqrt{2}a_C \times \sim 2a_C \times \sim\sqrt{2}a_C$, space group *Pnma*), which is sensitive to phase segregation. (a2)–(c2): ($I_0 = 0.005$) A multiplet containing the (1/2, 2, 2) peak, which has a large contribution from the structural distortions associated with the CO superstructure and a smaller magnetic contribution. (a3)–(c3): ($I_0 = 0.05$) A multiplet arising from the (1, 1, 1) peak of the pseudocubic cell, which is sensitive to ferromagnetic ordering. (a4)–(c4): ($I_0 = 0.03$) A region of the pattern containing three strong antiferromagnetic peaks. Crosses are experimental points (a few were omitted for clarity). Solid lines are calculated patterns from full-pattern Rietveld refinements. Dotted lines show the contributions of individual phases.

The powders were strongly compacted in a vanadium tube, and the absence of field-induced preferred orientation was experimentally confirmed. A few representative powder patterns, together with calculated profiles from full-pattern Rietveld refinements,[18] are shown in Fig. 1. At room temperature [Fig. 1(a1)–(a4)] the data are consistent with a single crystallographic phase, albeit associated with some anisotropic symmetric broadening, which accentuates on cooling to 200 K. At 150 K, we observed a dramatic change in the line shapes, which is preserved down to low temperatures. The new profiles [Fig. 1(b1)] are well represented by a two-phase model. However, in this context, the notion of crystallographic ''phases'' must be somewhat broadened to include a *continuous bimodal distribution* of lattice parameters, with significant intensity at intermediate values. The peak widths imply that these phases, both *structurally well distinct* from the room-temperature phase, are correlated at mesoscopic length scales (500–2000 Å). Characteristic superlattice Bragg peaks arising from CO [Fig. 1(b2)] are observed below 200 K, while magnetic peaks are consistent with a large AFM and a smaller FM contributions. The AFM and CO peaks can be attributed to one of the two crystallographic phases (labeled CO), both from an analysis of their *d* spacings and from the subsequent evolution as a function of magnetic field (see below). The attribution of the smaller FM component is more difficult, but it is likely to be associated with the second crystallographic phase (labeled ROO, for reverse orbital order; see below). At low temperatures, the CO an ROO phases occur in roughly equal proportions (Fig. 2). The line shape and the magnetic intensities undergo another major change upon application of the magnetic field [Fig. 1(c1)–(c4)]. Now, most of the intensity (85%) is associated with a new phase [labeled CD for charge-delocalized in (c1)], which is ferromagnetic (c3) and has yet different lattice constants. The remaining 15% of the sample is the residual CO phase (c1), with the CO (c2) and AFM (c4) peaks scaling accordingly. On warming, there is a first transition occurring at 40 K, whereby the proportions of CD and CO phases become almost equal, with a corresponding growth of the CO and AFM peaks (Fig. 2). This first transition is associated with the metal-insulator transition in resistivity. The remaining CD phases then transforms into the ROO phase with onset at 120 K, closing the hysteresis loop.

It is immediately clear that this pattern of phase coexistence is not consistent with electronic phase segregation. In fact, the two-phase behavior is first observed just below T_{CO}, associated with an *increase* in electrical resistivity. This is totally incompatible with the ROO phase being metallic, since its fraction is well above the percolation threshold. More information about the electronic nature of the coexisting phases can be gathered from their structural properties. However, since an unconstrained refinement of the individual internal coordinates is most likely unreliable, our analysis will be based only on lattice parameters, as extracted from two-phase Rietveld refinements. We have chosen two structural indicators. The first (''charge localization'') parameter is the unit cell volume, which is good indicator of charge delocalization.[19] The effect of temperature has been factored out by extrapolating all the volumes to zero temperature: $V_0 = V(T)/[E_{\mathrm{Debye}}(T,\Theta_D)\times\alpha_{\mathrm{vol}}+1]$, where $E_{\mathrm{Debye}}(T,\Theta_D)$ is the Debye lattice energy. Θ_D (the Debye temperature), and α_{vol} (the volume Grüneisen parameter) were chosen to be 600 K and 9.95×10^{-6}, respectively, by fitting the volume temperature dependence of the typical manganese perovskite $La_{0.75}Ca_{0.25}MnO_3$ above T_C and up to 800 K.[20] In the case of $La_{0.75}Ca_{0.25}MnO_3$, V_0 is constant above T_C and drops by about 0.3% below T_C due to charge delocalization. The second (''orbital order'') parameter is the unit cell anisotropy, $\nu = b/\sqrt{a^2+c^2}$ (*Pnma* space group setting), which sharply drops at T_{CO} in charge-ordered compounds such as $La_{0.5}Ca_{0.5}MnO_3$ due to preferential ordering

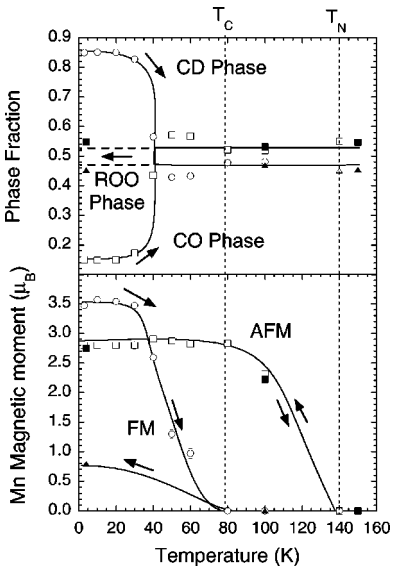

FIG. 2. Fractions and magnetism of the coexisting phases in $Pr_{0.7}Ca_{0.3}MnO_3$ from multiphase Rietveld refinements of neutron data. *Top*: phase fractions of the charge-ordered antiferromagnetic phase (squares), charge-delocalized ferromagnetic phase (circles) and reverse-orbital-ordered weakly ferromagnetic spin-glass phase (triangles) on zero-field cooling (filled symbols) and warming after 7 T field processing at 3 K (open symbols). Arrows indicate the direction of cooling/heating. *Bottom*: magnetic moments per manganese atom for the individual phases (symbols as in top panel). When not shown, error bars are smaller than the symbols. Lines are guides to the eyes.

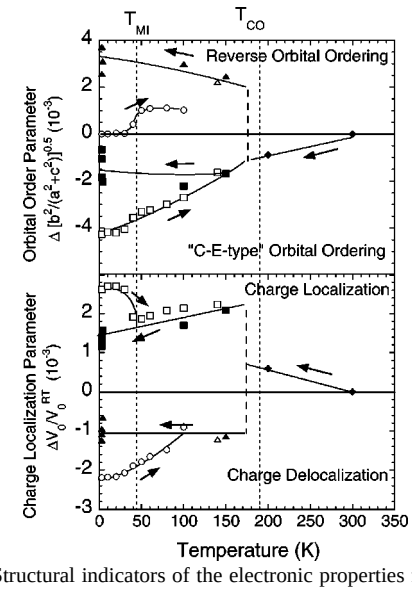

FIG. 3. Structural indicators of the electronic properties for the coexisting phases in $Pr_{0.7}Ca_{0.3}MnO_3$. *Bottom*: normalized differential ground state volume, a structural indicator of charge localization (see text). *Top*: Differential unit cell anisotropy, which indicates the degree of orbital ordering. Symbols are as in Fig. 2. Arrows indicate the direction of cooling (in zero field) or heating (after 7 T field processing).

of filled e_g orbitals in the *a-c* plane.[21] There is a close correspondence between these parameters and the line shapes shown in Fig. 1(a1)–(c1). Changes in ν affect the *splitting* of the 202-040 doublet (a decrease in ν will increase the splitting), while changes in V_0 affect its *position* (a decrease in V_0 moves the doublet to the left). The temperature dependence of the ''charge localization'' and ''orbital order'' parameters is shown in Fig. 3 (the room temperature values V_0^{RT} and ν^{RT} were subtracted,[22] and the volume was also divided by V_0^{RT}). The values for the CO and CD phases are clearly consistent with our previous knowledge of these phases: the CO phase is charge-localized (large volume) and shows conventional ''*C-E*-type'' orbital ordering (negative $\Delta\nu$=large splitting), whereas the CD phase has zero orbital ordering and small unit cell volume. It is noteworthy that the CO phase surviving after field processing shows more ''extreme'' structural characters, perhaps associated with greater stability. For the ROO phase, the volume parameters indicates an intermediate degree of localization, whereas the unit cell anisotropy is consistent with a larger-than-random proportion of the filled e_g orbitals being *perpendicular* to the *a-c* plane (*reverse* orbital ordering). A straightforward bond length calculation shows that the expected values of $\Delta\nu$, compatible with the overall stoichiometry, are -5×10^{-3} and $+7.4\times10^{-2}$ for fully ordered *C-E*-type-CO and ROO phases, respectively. Our observations are therefore consistent with a largely *ordered C-E* phase, confirmed by the large refined atomic shifts associated with the CO superstructure peaks [Fig. 1(c2)]. Conversely, the ROO phase is a largely *disordered* orbital ''glass'' with a small degree of preferential orbital ordering along the *b* axis. Both structural order parameters show opposite behavior in the ROO and CO phases. This immediately points to *intragranular strain* as a possible origin of CO-ROO phase coexistence, as previously suggested by Littlewood.[23] In this scenario, growing nuclei of the CO phase would apply stress to other regions of the same crystallite, effectively preventing them from transforming and favoring a reverse orbital arrangement. It is possible that these phases may be pinned to local chemical inhomogeneities, which would explain the difficulty in annealing one of them out after field processing and the pronounced sample dependence of some properties.

The mesoscopic phases we observed always have significant phase fractions, almost always above the percolation threshold. Therefore, the electronic properties must largely be determined at the microscopic level. There is therefore great interest in understanding if *microscopic* clustering phenomena occur, and how they relate to *mesoscopic* phase coexistence. We have studied the short-range spin static and dynamic correlations using QESANS. Data from the same powder sample used in the diffraction experiment were collected on warming at the IN5 chopper spectrometer at the Institut Laue-Langevin, using a 4.8 Å incident wavelength (no magnetic field was applied). For the determination of the diffusion constant, we only analyzed data from the small-angle detector, covering the momentum transfer range $0.04\,\text{Å}^{-1}\leqslant Q_{\mathrm{el}}\leqslant 0.136\,\text{Å}^{-1}$. The energy transfer window was ±2 meV. We also collected a smaller number of data sets on the D7 polarized-neutron diffractometer with polarization analysis ($0.15\ \text{Å}^{-1}\leqslant Q\leqslant 2.5\ \text{Å}^{-1}$), to unequivocally determine that the small-angle signal is of magnetic origin, and to obtain an absolute-scale normalization. Energy-integrated cross sections were fitted using the squared-Lorentzian spin correlation model proposed by Viret *et al.*,[24] yielding the short-range magnetic correlation length and the associated fraction of the magnetic moment per for-

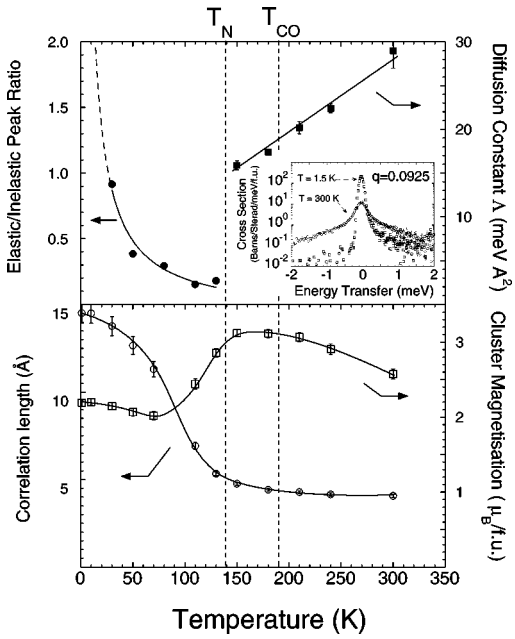

FIG. 4. Static and dynamic short-range magnetic properties of phase-segregated $Pr_{0.7}Ca_{0.3}MnO_3$. *Bottom*: Magnetic correlation length (open circles) and average magnetic moment per manganese ion (open squares) as a function of temperature, from fits of energy integrated SANS data (see text). *Top*: magnetic diffusion constant (extracted from Lorentzian full widths at half maximum) above the spin-glass temperature $T_{SG} \leqslant T_N$ (filled squares) and ratio between the elastic and the quasielastic integrated intensity ratio at $Q_{el}=0.05\ \text{Å}^{-1}$ below T_{SG} (filled circles). The *inset* shows representative inelastic data sets at 300 and 1.5 K (positive energies represent an energy *gain* for the sample). Lines are guides to the eyes.

mula unit (Fig. 4, bottom panel). Quasielastic data were first converted in Q-ω space, and then fitted at constant Q using the sum of a Lorentzian contribution and a delta-function convoluted with the resolution function of the instrument, taking into account the thermal population factor. Following Lynn *et al.*,[5] the Q dependence of the Lorentzian full width at half maximum was fitted with a quadratic law, yielding a magnetic ''diffusion constant'' (Fig. 4, upper panel). As in the case of ''conventional'' manganites, the correlation length increases with decreasing temperature, while the diffusion constant decreases, our data being in good quantitative agreement with previous literature.[5,25] Unlike the case of $La_{0.67}Ca_{0.33}MnO_3$ studied by Lynn *et al.*, $Pr_{0.7}Ca_{0.3}MnO_3$ never undergoes a spontaneous metal-insulator transition, which suppresses the small-angle magnetic scattering. In our data, therefore, the SANS is present down to the lowest temperatures. A pronounced drop is visible at T_N, where the average magnetic moment per manganese ion decreases to 66% of its original value, corresponding to 57% of the spins no longer contributing to the SANS. This is in excellent agreement with the phase fraction of the CO phase, for which the moments become long-range ordered. It is therefore likely that, below 100 K, only the ROO phase contributes to the SANS. In addition, the elastic contribution to the QESANS spectra starts to increase below 140 K, until, at low temperatures, the signal is mostly elastic (Fig. 4, inset). This behavior is similar to that observed in classic spin-glass systems,[26] suggesting that the ROO phase behave like a ferromagnetic cluster glass, with $T_{SG} \leqslant T_N$. This interpretation is consistent with the ''orbital glass'' structural nature of the ROO phase.

In conclusion, we have studied the phase coexistence at both microscopic (5–20 Å) and mesoscopic (500–2000 Å) scales in $Pr_{0.7}Ca_{0.3}MnO_3$. The structural characters of the mesoscopic phases point to intragranular strain as the main driving force for phase segregation. Ferromagnetic short-range correlations, previously taken as evidence of microscopic phase segregation, occur in both phases at high temperatures, but are restricted to the ROO phase at low temperatures, since the spins of the CO phase display long-range AFM order. The short-range spin dynamics at low temperature is strongly reminiscent of spin glass behavior.

We acknowledge the invaluable help we received from Amir Murani, who discussed with us the interpretation of the QESANS. We also acknowledge the help of the ILL and ISIS technical staff, and we are particularly grateful to J. Chauhan and D. F. Bates for their help in the complex HRPD cryomagnet experiment. The work of D.N.A. and I.F.M. was supported by the U.S. Department of Energy, Basic Energy Sciences-Materials Sciences, under Contract No. W-31-109-ENG-38. S.W.C. is partially supported by Grant No. NSF-DMR-9802513.

*Present address: ISIS facility, Rutherford Appleton Laboratory-CCLRC, Chilton, Didcot, Oxfordshire, OX11 0QX, U.K.

[1] P.-G. de Gennes, Phys. Rev. **118**, 141 (1960).
[2] A. Moreo *et al.*, Science **283**, 2034 (1999).
[3] S. Yunoki *et al.*, Phys. Rev. Lett. **80**, 845 (1998).
[4] A. J. Millis *et al.*, Phys. Rev. Lett. **77**, 175 (1996).
[5] J. W. Lynn *et al.*, Phys. Rev. Lett. **76**, 4046 (1996).
[6] J. M. De Teresa *et al.*, Nature (London) **386**, 256 (1997).
[7] H. Y. Hwang *et al.*, Phys. Rev. Lett. **75**, 914 (1995).
[8] D. E. Cox *et al.*, Phys. Rev. B **57**, 3305 (1998).
[9] M. Uehara *et al.*, Nature (London) **399**, 560 (1999).
[10] D. N. Argyriou *et al.*, Phys. Rev. B **61**, 15 269 (2000).
[11] S. Katano *et al.*, Physica B **276**, 786 (2000).
[12] Z. Jirák *et al.*, J. Magn. Magn. Mater. **53**, 153 (1985).
[13] H. Y. Hwang *et al.*, Phys. Rev. B **52**, 15 046 (1995).
[14] H. Yoshizawa *et al.*, J. Phys. Soc. Jpn. **65**, 1043 (1996).
[15] Y. Tomioka *et al.*, Phys. Rev. B **53**, R1689 (1996).
[16] V. Kiryukhin *et al.*, Nature (London) **386**, 813 (1997).
[17] A. M. Balagurov *et al.*, Phys. Rev. B **60**, 383 (1999).
[18] A. C. Larson and R. B. von Dreele, *General Structure Analysis System* (The Regents of the University of California, Los Alamos, 1985).
[19] P. G. Radaelli *et al.*, Phys. Rev. Lett. **75**, 4488 (1995).
[20] P. G. Radaelli *et al.*, Phys. Rev. B **56**, 8265 (1997).
[21] P. G. Radaelli *et al.*, Phys. Rev. B **55**, 3015 (1997).
[22] Independently on orbital ordering, octahedral tilts also contribute to the parameter v, as clearly evident from the room-temperature splitting of the 202-040 doublet. This contribution depends on composition, but is only weakly temperature-dependent.
[23] P. B. Littlewood, Nature (London) **399**, 529 (1999).
[24] M. Viret *et al.*, Phys. Rev. B **55**, 8067 (1997).
[25] R. Kajimoto *et al.*, Phys. Rev. B **58**, 11837 (1998).
[26] A. P. Murani, J. Magn. Magn. Mater. **22**, 271 (1981).